

Thermal vesiculation during volcanic eruptions

Yan Lavallée^{1*}, Donald B. Dingwell², Jeffrey B. Johnson³, Corrado Cimarelli²,
Adrian J. Hornby¹, Jackie E. Kendrick¹, Felix W. von Aulock¹, Ben M. Kennedy⁴,
Benjamin J. Andrews⁵, Fabian B. Wadsworth^{1,2}, Emma Rhodes⁴, Gustavo Chigna⁶

¹ Department of Earth, Ocean and Ecological Sciences, University of Liverpool,
Liverpool L69 3GP, UK

² Department of Earth and Environmental Sciences, Ludwig Maximilian University of
Munich, Theresienstrasse 41/III, 80333 Munich, Germany

³ Department of Geosciences, Boise State University, Boise, Idaho, USA

⁴ Geological Sciences, University of Canterbury, Private Bag 4800, 8140
Christchurch, New Zealand

⁵ Department of Mineral Sciences, Smithsonian Institution, Washington, District of
Columbia, USA

⁶ Instituto Nacional de Sismologia, Vulcanologia, Meteorologia, e Hydrologia
(INSIVUMEH), 7a Avenue 14-57, Zone 13, Guatemala City, Guatemala

*Corresponding author: Department of Earth, Ocean and Ecological Sciences,
University of Liverpool, Liverpool L69 3GP, UK (Yan.Lavallee@liverpool.ac.uk)

Terrestrial volcanic eruptions are the consequence of magmas ascending to the surface of the Earth. This ascent is driven by buoyancy forces, which are enhanced by the exsolution and suspension of magmatic volatiles that reduce the density of magma¹. The development of vesicularity also greatly reduces the *strength* of magma², a material parameter controlling fragmentation and thus explosive potential³. To date, the development of vesicularity in magmas has been viewed (both thermodynamically and kinetically) in terms of the pressure dependence of the solubility of water in the magma, and its role in driving gas saturation, exsolution and expansion during decompression. In stark contrast, consideration of any volcanic impact of the well-documented negative temperature-dependence of solubility has been largely ignored. Recently, petrological constraints have demonstrated that significant heating of magma may indeed be a common result of the latent heat of crystallisation⁴ as well as viscous^{5,6} and frictional⁷ heating in areas of strain localisation. Here, we present clear evidence, from both field and experimental observations, of magma vesiculation and fragmentation resulting from heating (rather than decompression). Textural analysis of volcanic ash from Santiaguito (Guatemala) reveals the presence of chemically heterogeneous filaments hosting micro-vesicles. The textures mirror those developed by disequilibrium melting induced via rapid heating during fault friction experiments, demonstrating that friction can generate sufficient heat to induce melting and vesiculation of hydrated silicic magma. Remarkably, consideration of the experimentally-determined temperature- and pressure-dependence of water solubility reveals that, for many ascent paths, exsolution may be more efficiently achieved by heating than by decompression. We conclude that the thermal path experienced by magma during ascent is a first-order control on degassing, vesiculation, magma strength and the effusive-explosive transition in volcanic eruptions.

Volcanic eruptions result from magma buoyancy, largely powered by volatile exsolution. In standard models of magma ascent this exsolution is triggered by decompression^{8,9}. Upon ascent, gas bubbles expand and pressure build-up may precipitate fragmentation and explosive eruption¹. Yet the solubility, which sets the thermodynamic driving force for saturation and vesiculation in a volatile component has long been known to be a function of temperature as well¹⁰. Thus temperature changes may also generate magma vesiculation. Despite this, to date, no models of volcanic eruptions have explored the role of temperature in generating magmatic vesicularity.

The thermal evolution of magma in volcanic conduits has received increased attention in recent years. Firstly, petrological studies have demonstrated that crystallising magmas can heat up significantly (*e.g.*, ~100 °C) due to the latent heat liberated⁴ - a process acting across the entire magmatic column. Secondly, zones in which magma undergoes strain localisation during ascent also exhibit evidence of significant heating (up to ~250 °C) resulting from viscous energy dissipation^{5,6,11,12}. Thirdly, the discovery of pseudotachylytes in erupted dome rocks¹³ and at the margin of lava spines⁷ indicates that fault friction can be an important contributor to the thermal budget of magma (locally up to ~1000 °C), exercising as a result a first-order control on volcanic eruption dynamics¹⁴.

Evidence is mounting that magma ascent may commonly be controlled by strain localisation near conduit margins¹⁵. Such strain localisation in magmas has been proposed as a scenario leading to failure and potentially serving as a trigger for explosive eruptions^{16,17}. Careful examination of shallow volcanic conduit structures lends support to these proposals¹⁸. Magmatic conduits/dykes are relatively narrow (tens of centimetres to a few meters) at depths of a few kilometres¹⁹, thus regions of strain localisation may represent an important mass fraction of ascending magma. At shallow depths, where conduits can be wider (meters to a few tens of meters), areas of strain localisation may not appear to be inevitable, yet the observation that shallow magma bodies are heavily fractured²⁰, and the influence of such fractures on surficial magma behaviour²¹ suggest that strain localisation and its associated heat, may play a large role throughout the whole length of the magmatic column.

Estimates of magma ascent rates vary widely. In general, explosive eruptions have been associated with high ascent rates, reaching up to a few meters per second prior to fragmentation⁹. During such rapid ascent, magma decompresses (1 m.s⁻¹ corresponds to decompression of 0.02 MPa.s⁻¹); simultaneously heat is generated in all areas where strain is localised, either by fault friction¹⁴ or viscous dissipation¹². The material record of such heat may or may not be documented in the products of the subsequent volcanic explosions. The mineralogical assemblage can often preserve information related to such heating^{7,13}, but if sufficient time is available then the assemblage will recover in response to the mean temperature and pressure conditions and evidence of fluctuations may be lost. The glassy state itself does not provide direct information from above the glass transition temperature; yet, indirectly, evidence of energy dissipation has been inferred from the morphology of the porous network preserved in glassy volcanic products^{5,6}. Difficulty of preservation of evidence of heating in ascending magma, or indeed of the temperature history, is likely a major reason for its neglect in eruption models.

Temperature and pressure both affect the solubility of water²²⁻²⁴ (the dominant volatile component of volcanic activity) in magma. For a calc-alkaline rhyolitic melt, the temperature- and pressure-dependence of water solubility can be estimated by²⁴:

$$H_2O_t = \frac{354.94P^{0.5} + 9.623P - 1.5223P^{1.5}}{T} + 0.0012439P^{1.5} \quad (1),$$

where H_2O_t is total dissolved H_2O content (in wt.%), T is temperature (in K), and P is pressure (in MPa). Figure 1a shows that due to the strongly retrograde nature of the H_2O solubility curve at low pressures, an increase in temperature is a driving force for vesiculation in this pressure range. This temperature-dependence is evidently large enough to have a significant effect on water saturation during magma ascent in conduits.

The potential magnitude of water exsolution (ΔH_2O) due to 1) decompression and 2) heating is analysed here at a magmatic temperature of 850 °C (Figure 1b). The comparison of the individual effects of decompression versus heating yields striking results. We find that heating events of hundreds of degrees, as described above, are a first-order driving force for significant exsolution and vesiculation. For an ascent rate of 1 m.s⁻¹ (*i.e.*, 0.02 MPa.s⁻¹, capable of triggering explosive events), 1 K of heating has the potential to generate more water exsolution than 0.02 MPa of decompression from initial pressures greater than 13 MPa (Figure 1c); and further heating can be the main driving force for vesiculation. Expressing it in a different way, a decompression event exceeding 0.1 MPa (>5 m) would be required in order to exsolve more water than that exsolved by 1 °C of heating. We therefore conclude from this analysis that the thermal path of decompressing magma can significantly influence volatile exsolution. It is thus easy to envisage scenarios of heating-dominated or “thermal” vesiculation during magma ascent at moderate pressures, and below we provide evidence to support the assertion that such thermal exsolution also dominates during strain localisation in magma at shallower depths.

We have examined eruptive products at the Santiaguito dome complex. The active Caliente lava dome offers one of the most spectacular displays of cyclic, piston-like eruptive activity ever recorded, commonly climaxing in gas-and-ash explosions along concentric fractures^{21,25,26} (Figure 2a). Proximal monitoring of this dome has revealed a regular (~26-minute) periodicity in ground inflation/deflation cycles²⁷. At the expansion maxima, the propagation of arcuate faults across the dome’s surface is observed and the dome’s centre thrusts upward and collapses back, followed by dome deflation²¹. Gas-and-ash explosions occur episodically along the faults, coincident with very-long-period (VLP) seismic events, which have been interpreted to be associated with gas flow in fractures at the inflation maximum (Figure 2b)²⁷. In the analysis that follows, the rates of inflation and deflation during ash release and the magnitude and rate of slip are of central importance. Ash ejection only occurs during the fastest inflation/deflation cycles (Figure 2b)²⁷. In these cases, the arcuate faults undergo a metre of uplift and collapse within 1 second, corresponding to a slip rate of <2 m.s⁻¹ (21). Importantly, these lava dome dynamics leave scars on the blocks forming the dome carapace, with frictional marks preserved as both striations and slickensides.

Textural examination of volcanic ash collected upon deposition in November 2012 and November 2014 provides several examples of the material consequences of such frictional processes (Supplementary Figures 1-4). The interstitial glass phase reveal a juxtaposition of chemically distinct mingled filaments with different shades of grey

on back-scattered electron (BSE) images obtained by scanning electron microscopy (SEM; Figure 2c; Supplementary Figure 3-4). The contacts between the light- and darker-toned filaments are diffuse and fluidal (unlike crystals with sharp and angular boundaries). The very fine nature of these filaments and the diffuse boundaries prevent us from using standard geochemical analysis techniques accurately, but the greyscale values observed (which reflect the atomic number and thus chemical variations within and between phases) provide clear evidence of chemical heterogeneity (Figure 2c; Supplementary Figure 4). These melt phases have evidently mingled with the original interstitial melt on timescales insufficient for homogenisation, presumably immediately before the fragmentation and eruption that locked in these dynamic features.

The mingling textures exhibited by the Caliente ash mirror those of protomelts resulting from selective melting of individual crystals that have been observed in the products of frictional melting experiments^{28,29}. Such experiments involve an extremely rapid heating rate ($>10^3$ to 10^4 °C.s⁻¹) and therefore highly disequilibrium melting induced by fault friction²⁸⁻³⁰. We propose here that the Caliente ash samples contain volcanic pseudotachyte; evidence of the syn-eruptive operation of frictional heating sufficient to generate melting in the piston-like events at Caliente dome. Notably, the protomelts present in the ash contain vesicles (as indicated by blue arrows on Figure 2c). As the crystalline phases present are anhydrous and thus cannot serve as a source of water for vesiculation, we suggest that vesiculation took place in the interstitial melt. If so, these frictional melts contain what may be the first well-documented evidence of thermal vesiculation in volcanic products.

As an experimental demonstration of the feasibility of thermal vesiculation, we have performed fault friction experiments at conditions designed to simulate the piston-like gas-and-ash explosion events at Caliente²¹. During the experiment the flat ends of two hollow, cylindrical cores of a Caliente dome rock were pushed together at an applied normal stress of 6 MPa (representative of the depth of tilt and seismic sources²⁷) and one core was rotated (against the other) at an equivalent velocity of 1 m.s⁻¹ (see online Supplementary section and Supplementary Figure 5). Friction experiments on magmas have shown that under such conditions frictional melting takes place within as little as ~ 10 cm of slip^{13,14,28} confirming the feasibility of this process.

As noted above, microscopic inspection of the fault products experimentally generated in the Caliente dome rock reveals the presence of multiple, chemically heterogeneous melt filaments extruded from crystals adjacent to the fault zones (Figure 2d; Supplementary Figure 6). In addition, we note that the interstitial glass of the host rock in the first 0.3-0.4 mm near the fault zone has partially vesiculated (Figure 2e; Supplementary Figure 7). To ensure that vesiculation resulted from substantial heat near the fault zone, we have tested the stability of dissolved water in this dome rock at background magmatic temperature by subjecting two small cores to 850 °C for 30 minutes and 15 hours, respectively. We observe that no water exsolved to form vesicles, even after a 15 hour dwell (Supplementary Figure 8). We conclude from these experiments that both the generation of crystal protomelts and the surrounding vesiculation result directly from the frictional work converted to significant heat during faulting events, and not due to residence at magmatic temperature. From the similarity of these experimental products of frictional melting to the natural samples of Caliente (described above) we deduce that the cyclic

phenomena observed during dome extrusion and explosions at Caliente occur in the presence of strain localisation, accompanied by thermal vesiculation.

The occurrence of superheated vesiculation at Caliente can be assessed by modelling the conversion of mechanical work to heat (ΔT) during friction, using³¹:

$$\Delta T = \frac{\mu \sigma_n V \sqrt{t}}{\rho C_p \sqrt{\pi k}} \quad (2).$$

Considering Byerlee's friction coefficient (μ) of 0.85 (at static conditions), a normal stress (σ_n) of 6 MPa⁽²⁷⁾, a slip velocity (V) of 1 m.s⁻¹ for a duration (t) of 0.5 s⁽²¹⁾, a density (ρ) of 2,630 kg.m⁻³ (by He-pycnometry), a specific heat capacity (C_p) of 900 J.kg⁻¹.K⁻¹, and a thermal diffusivity (k) of 10⁻⁶ m².s⁻¹, uplift of the dome would generate a local temperature increase of 860 °C along the arcuate faults. Given that the magma already resides at ~850 °C⁽³²⁾, and that experimental work has shown that only moderate temperature increase occurs once frictional melt lubricates a slip zone^{13,14,28}, temperature would not be expected to significantly exceed the melting temperatures of the main rock-forming minerals in the Caliente lava (labradorite and enstatite, which melt at >1300 and >1400 °C respectively³⁰). This magnitude of heating would induce water exsolution from the melt in zones of strain localisation. Due to the current eruptive cycles and outgassing activity at Caliente, we consider the system to be open to an extent that allows for exsolution of any oversaturated volatile fraction; thus a total of 0.83 wt. % would be expected to remain in the magma at the point of fragmentation at 6 MPa (Figure 1a). Heating of ~550-860 °C would induce a dramatic oversaturation in water of 0.26-0.35 wt. %. Faulting, creation of new surface area, and forced convection during frictional melting would all serve to minimise effective diffusion path lengths and enhance the completion of water exsolution. With such overheating, and thus heightened H₂O diffusivity, the kinetic limitation to vesiculation (nucleation and growth) should also be easily overcome, promoting foaming. At a depth of ~300 metres such vesiculation would, in turn, reduce the strength of magma and thereby trigger fragmentation³³. We therefore conclude that vesiculation can be induced by rapid heating in the conduit.

Water is central to magma ascent dynamics and its contribution to magmatic and volcanic processes results from a combination of both pressure and temperature. Decompression is inevitable and acts throughout magma ascent. Here we argue that heating via both crystallisation and shearing processes are equally inevitable. More specifically, the magnitude of viscous and frictional heating may be prodigious, and thus exert a primary control on volatile exsolution. At the rates and magnitudes of heating discussed here, the solubility of water in a melt should be affected before heat loss by thermal conductivity to the cooler surroundings – whether in the core of the magmatic column (where further water may exsolve) or in the country rock – could serve to counteract local heating. Heating during magma ascent deserves adequate consideration in conduit transport and eruption models.

The fact that temperature may dominate the dynamics of water saturation and vesiculation during magma transport in volcanic conduits is a wholly novel constraint. Clearly, efforts must be made to better constrain the thermal path of magmas during ascent. A thorough reassessment of strain localisation across deep dykes and shallow conduits should lead to the quantification of shear heating during magma transport. As a balance of heating and decompression dictates the driving force for degassing, the physico-chemical factors which ultimately control the explosivity of volcanic

- events need to be re-evaluated in light of this. We now urge further development of this important concept in the simulation and analysis of magma ascent and eruption.
- 1 Sahagian, D. Volcanology - Magma fragmentation in eruptions. *Nature* **402**, 589-+ (1999).
 - 2 Vasseur, J., Wadsworth, F. B., Lavallée, Y., Hess, K.-U. & Dingwell, D. B. Volcanic sintering: Timescales of viscous densification and strength recovery. *Geophysical Research Letters* **40**, 5658-5664, doi:10.1002/2013gl058105 (2013).
 - 3 Dingwell, D. B. Volcanic dilemma: flow or blow? *Science* **273**, 1054-1055 (1996).
 - 4 Blundy, J., Cashman, K. & Humphreys, M. Magma heating by decompression-driven crystallization beneath andesite volcanoes. *Nature* **443**, 76-80, doi:10.1038/nature05100 (2006).
 - 5 Rosi, M., Landi, P., Polacci, M., Di Muro, A. & Zandomenighi, D. Role of conduit shear on ascent of the crystal-rich magma feeding the 800-year-BP Plinian eruption of Quilotoa Volcano (Ecuador). *Bulletin of Volcanology* **66**, 307-321 (2004).
 - 6 Wright, H. M. N. & Weinberg, R. F. Strain localization in vesicular magma: Implications for rheology and fragmentation. *Geology* **37**, 1023-1026, doi:10.1130/g30199a.1 (2009).
 - 7 Kendrick, J. E. *et al.* Extreme frictional processes in the volcanic conduit of Mount St. Helens (USA) during the 2004-2008 eruption. *Journal of Structural Geology* **38**, 61-76, doi:10.1016/j.jsg.2011.10.003 (2012).
 - 8 Martel, C. & Schmidt, B. C. Decompression experiments as an insight into ascent rates of silicic magmas. *Contributions to Mineralogy and Petrology* **144**, 397-415, doi:10.1007/s00410-002-0404-3 (2003).
 - 9 Proussevitch, A. A. & Sahagian, D. L. Dynamics and energetics of bubble growth in magmas: Analytical formulation and numerical modeling. *Journal of Geophysical Research-Solid Earth* **103**, 18223-18251, doi:10.1029/98jb00906 (1998).
 - 10 Ghiorso, M. S. & Sack, R. O. Chemical mass-transfer in magmatic processes .4. A revised and internally consistent thermodynamic model for the interpolation and extrapolation of liquid-solid equilibria in magmatic systems at elevated temperatures and pressures. *Contributions to Mineralogy and Petrology* **119**, 197-212, doi:10.1007/bf00307281 (1995).
 - 11 Hess, K. U., Cordonnier, B., Lavallée, Y. & Dingwell, D. B. Viscous heating in rhyolite: an in situ determination. *Earth and Planetary Science Letters* **275**, 121-126 (2008).
 - 12 Mastin, L. G. The controlling effect of viscous dissipation on magma flow in silicic conduits. *Journal of Volcanology and Geothermal Research* **143**, 17-28 (2005).
 - 13 Kendrick, J. E. *et al.* Seismogenic frictional melting in the magmatic column. *Solid Earth* **5**, 199-208, doi:10.5194/se-5-199-2014, 2014 (2014).
 - 14 Kendrick, J. E. *et al.* Volcanic drumbeat seismicity caused by stick-slip motion and magmatic frictional melting. *Nature Geoscience* **7**, 438-442, doi:10.1038/ngeo2146 (2014).
 - 15 Lavallée, Y., Hess, K.-U., Cordonnier, B. & Dingwell, D. B. Non-Newtonian rheological law for highly crystalline dome lavas. *Geology* **35**, 843-846, doi:10.1130/g23594a.1 (2007).
 - 16 Gonnermann, H. M. & Manga, M. Explosive volcanism may not be an inevitable consequence of magma fragmentation. *Nature* **426**, 432-435 (2003).

- 304 17 Papale, P. Strain-induced magma fragmentation in explosive eruptions. *Nature*
305 **397**, 425-428 (1999).
- 306 18 Tuffen, H., Dingwell, D. B. & Pinkerton, H. Repeated fracture and healing of
307 silicic magma generate flow banding and earthquakes? *Geology* **31**, 1089-
308 1092 (2003).
- 309 19 Noguchi, S., Toramaru, A. & Nakada, S. Groundmass crystallization in dacite
310 dykes taken in Unzen scientific drilling project (USDP-4). *Journal of*
311 *Volcanology and Geothermal Research* **175**, 71-81,
312 doi:10.1016/j.jvolgeores.2008.03.037 (2008).
- 313 20 Stasiuk, M. V. *et al.* Degassing during magma ascent in the Mule Creek vent
314 (USA). *Bulletin of Volcanology* **58**, 117-130 (1996).
- 315 21 Johnson, J. B., Lees, J. M., Gerst, A., Sahagian, D. & Varley, N. Long-period
316 earthquakes and co-eruptive dome inflation seen with particle image
317 velocimetry. *Nature* **456**, 377-381, doi:10.1038/nature07429 (2008).
- 318 22 Holtz, F., Behrens, H., Dingwell, D. B. & Johannes, W. H₂O solubility in
319 haplogranitic melts - compositional, pressure and temperature-dependence.
320 *American Mineralogist* **80**, 94-108 (1995).
- 321 23 Ryan, A. G., Russell, J. K., Nichols, A. R. L., Hess, K.-U. & Porritt, L. A.
322 Experiments and models on H₂O retrograde solubility in volcanic systems.
323 *American Mineralogist* **100**, 774-786, doi:10.2138/am-2015-5030 (2015).
- 324 24 Liu, Y., Zhang, Y. X. & Behrens, H. Solubility of H₂O in rhyolitic melts at
325 low pressures and a new empirical model for mixed H₂O-CO₂ solubility in
326 rhyolitic melts. *Journal of Volcanology and Geothermal Research* **143**, 219-
327 235, doi:10.1016/j.jvolgeores.2004.09.019 (2005).
- 328 25 Holland, A. S. P., Watson, I. M., Phillips, J. C., Caricchi, L. & Dalton, M. P.
329 Degassing processes during lava dome growth: Insights from Santiaguito lava
330 dome, Guatemala. *Journal of Volcanology and Geothermal Research* **202**,
331 153-166, doi:10.1016/j.jvolgeores.2011.02.004 (2011).
- 332 26 Scharff, L., Hort, M. & Gerst, A. The dynamics of the dome at Santiaguito
333 volcano, Guatemala. *Geophysical Journal International*, 1-17,
334 doi:10.1093/gji/ggu069 (2014).
- 335 27 Johnson, J. B., Lyons, J. J., Andrews, B. J. & Lees, J. M. Explosive dome
336 eruptions modulated by periodic gas-driven inflation. *Geophysical Research*
337 *Letters* **41**, doi:10.1002/2014GL061310 (2014).
- 338 28 Hornby, A. J. *et al.* Spine growth and seismogenic faulting at Mt. Unzen,
339 Japan. *Journal of Geophysical Research: Solid Earth*, 2169-9356,
340 doi:10.1002/2014JB011660 (2015).
- 341 29 Lin, A. M. & Shimamoto, T. Selective melting processes as inferred from
342 experimentally generated pseudotachylytes. *Journal of Asian Earth Sciences*
343 **16**, 533-545 (1998).
- 344 30 Spray, J. G. in *Annual Review of Earth and Planetary Sciences, Vol 38* Vol. 38
345 *Annual Review of Earth and Planetary Sciences* (ed R. Freeman K. H.
346 Jeanloz) 221-254 (2010).
- 347 31 Carslaw, H. S. & Jaeger, J. C. *Conduction of Heat in Solids*. 2nd edn, (Oxford
348 University Press, 1959).
- 349 32 Harris, A. J. L. & Flynn, L. P. The thermal stealth flows of Santiaguito dome,
350 Guatemala: Implications for the cooling and emplacement of dacitic block-
351 lava flows. *Geological Society of America Bulletin* **114**, 533-546,
352 doi:10.1130/0016-7606(2002)114<0533:ttsfos>2.0.co;2 (2002).
- 353 33 Zhang, Y. X. A criterion for the fragmentation of bubbly magma based on
354 brittle failure theory. *Nature* **402**, 648-650, doi:10.1038/45210 (1999).
- 355

Supplementary Information is linked to the online version of the paper at www.nature.com/nature.

Acknowledgement

We thank Armando Pineda, the staff at INSIVUMEH and the Policia Nacional Civil de Guatemala for support with the field campaign. This work was supported by the European Research Council Starting Grant to Y.L. on *Strain Localisation in Magmas* (SLiM, No. 306488) and Advanced Grant to D.B.D. on *Explosive volcanism in the Earth system* (EVOKES, No. 247076). J.B.J. acknowledges the National Science Foundation EAR-grant No. 1151662. This work was partially funded the European Union's seventh program for research, technological development, and demonstration under grant agreement 282759 (VUELCO), and by the AXA Grant "Risk from Volcanic Ash in the Earth System". We are grateful to Dr. K. Genereau and Dr. L. Mastin for constructive reviews of this study.

Author Contributions

Y.L., J.E.K., F.W.v.A., A.J.H., F.B.W., B.J.A., B.M.K. and D.B.D. conceptualised the model. G.C. facilitated fieldwork and supported data analysis. Y.L., C.C., F.B.W., A.J.H., B.M.K., and E.R. performed fieldwork, collected samples and Y.L., F.W.v.A., A.J.H. and J.E.K. analysed the ash. A.J.H., J.E.K. and Y.L. performed the experiments. J.B.J. performed the geophysical analysis. All authors contributed to the manuscript.

Author Information Reprints and permissions information is available at www.nature.com/reprints. The authors declare no competing financial interests. Correspondence and requests for materials should be addressed to Y.L. (Yan.Lavallee@liverpool.ac.uk).

Figure Legends

Figure 1. Water concentration in rhyolitic magmas. a) Thermobarometric limits on water concentration²⁴ show that the heat induced by mechanical work (orange arrows) during magma ascent causes a decrease in water solubility (ΔH_2O). This decrease in concentration may be related to an equivalent decompression ($\sim \Delta P$). At Santiaguito, thermal input of, for example, ~ 600 °C due to short-lived faulting events may reduce water solubility by 0.28 wt.%. b) Water exsolution (ΔH_2O) driven by thermal input (red curves) vs decompression events (blue curves) for an ascending magma at a nominal temperature of 850 °C. These heating and decompression events are computed as a function of melt pressure at which the event initiates in the magmatic column. c) Fraction of the total water concentration exsolved from the action of heat (left y-axis), versus that of decompression (right y-axis) for different decompression and heating events. The data shows that thermal input (which acts on a timescale of seconds) generally induces more water exsolution than decompression.

Figure 2. Explosive eruptions caused by superheated vesiculation. a) Gas-and-ash explosion occurring along an arcuate fault on 10 November 2012 at Caliente dome, Santiaguito. b) Seismic signals (upper) and tilt data (lower) for explosive (red) and non-explosive (blue) inflation/deflation cycles associated with piston-like dynamics at Santiaguito²⁷. The solid lines display the average of the 26-minute cycles over the five-day long dataset, whereas the shaded areas exhibit the spread in the data. Gas-and-ash explosion cycles markedly differ from non-explosive cycles and are characterised by faster and stronger inflation/deflation as well as very long period (VLP) seismic events. c) BSE images showing heterogeneous protomelt filaments (yellow arrows) with different greyscale values (*i.e.*, a proxy for chemistry) extruded from crystals present in a volcanic ash particle sampled on 12 November 2012; some protomelts host vesicles (blue arrows). d) BSE images showing the shearing of protomelts near the main frictional melt zone (FMZ) produced experimentally by fault slip. e) BSE image showing vesiculation of the interstitial melt near the experimental fault zone due to high local temperature.

Figure 1

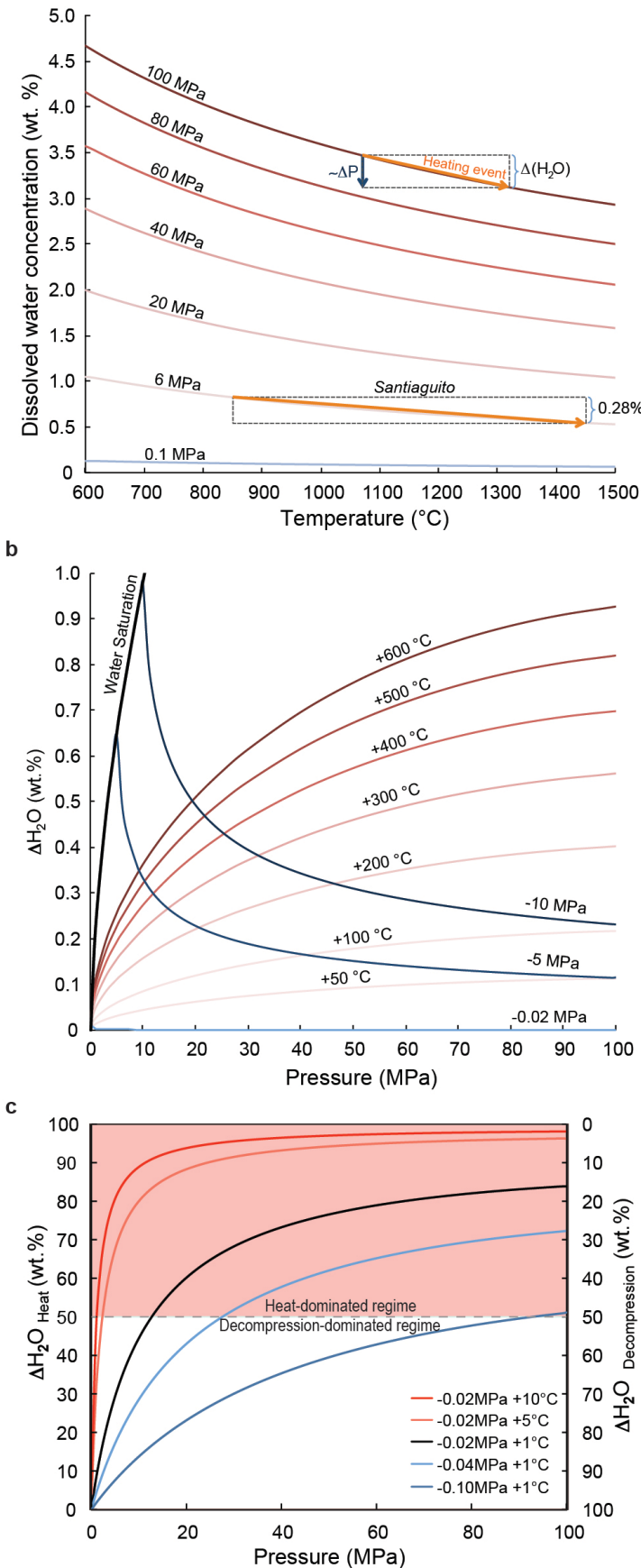
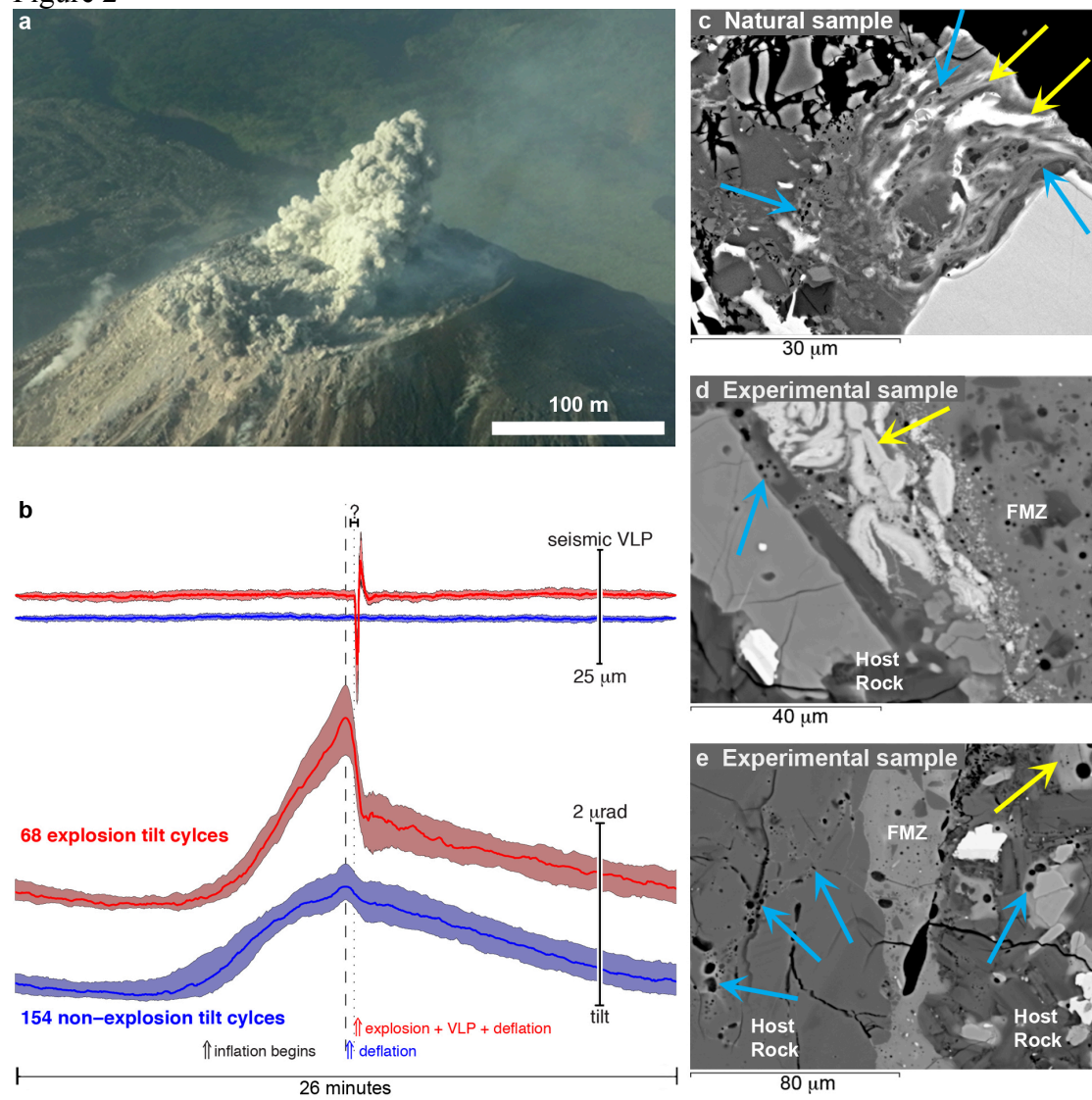


Figure 2



METHODS (online)**Volcanic ash sampling and analysis**

The ash samples were collected after each explosions from a location (14°44'35.11"N 91°33'40.69"W) approximately 275 m ENE from the active Caliente vent. The ash was collected by spreading a clean, 1.4 m x 1.4 m synthetic sheet. We used a paintbrush to carefully brush deposited ash into sample bags. The sheets were thoroughly cleaned after each sample collection and laid out to collect the ash of subsequent events. Due to the proximity of the sampling location, we are very confident of the source and timing of the ash employed in this study.

The grain size of the sampled volcanic ash was measured using a laser diffraction particle size analyser from Coulter. The density was determined on 25-mm diameter and 50-mm long rock cores using a 100cc helium pycnometer from Micromeritics.

Scanning electron microscopic analysis and energy-dispersive x-ray spectroscopy

Geochemical mapping across the natural samples and the experimental products was conducted in a Phillips XL 30 SEM using back-scattered electron (BSE) and energy-dispersive x-ray spectroscopy (EDS) run on the Oxford Instruments INCA software. BSE images provide an excellent means to identify frictional melting textures as the grey value of each phase relates to the atomic number, or density of major elements representing the geochemical composition³⁴. A dense phase consisting of heavy elements elastically reflects more electrons and thus shows up in light grey on a BSE image; conversely, an elementally light phase shows up in dark grey.

EDS was used to map the chemical concentration of major elements present in the different phases observed by BSE imaging. The EDS system allows mapping of the distribution of these elements across the main phases. We employed an electron beam of 5.5 µm at 20 keV and 8 nA. For the purpose of this study, we monitored the distribution of Si, Mg, Fe, Ti, Na and Al. Comparison of BSE and EDS images verify that the filaments have different chemical compositions.

Electron probe micro-analysis

Geochemical analysis of the phases present in the natural samples and the experimental products was performed in a CAMECA SX 100 Electron Probe Micro Analyser (EMPA) at the Ludwig Maximilian University of Munich (Germany). Probing of the glass and mineral phases was done using a focussed electron beam of 15 keV and 20 nA (Supplementary Figure 6). [Note that by using a focused beam on glass, the measured concentration of the alkalis, namely Na and K, are reduced by some 0.1-0.3 wt.% from what is likely to be present, however the filaments were too thin to be measured with a defocused beam, which would yield higher inaccuracy. Despite this, the results reveal the chemical distinction between the different phases.] In Supplementary Figure 6, we only present the chemical composition of the primary minerals and glass as well as that of the protomelts and main frictional melt from the experiments, as the phases were large enough to be analysed. In the natural ash, the filaments are rarely larger than 1 µm (see Supplementary Figure 2-4) and as such, EMP analysis was impracticable without a significant degree of contamination from surrounding phases, hence we used the greyscale in BSE images as well as EDS elemental maps to verify the occurrence of the same processes as observed in the experimental samples.

Fault slip experiments

The friction experiment was conducted in a low- to high-velocity rotary shear apparatus at the University of Liverpool, designed by T. Shimamoto and built by Marui, Japan. The experiment was conducted on two hollow, cylindrical samples with outer and inner diameters of 24.99 mm and 15.86 mm, respectively (Supplementary Figure 5). The samples were axially loaded using an air actuator at a normal stress of 6.0 MPa, as constrained by the depth of seismicity, and slip was applied on one rotating sample via a servo motor operated at 1200 rotations per minute, to induce an equivalent slip rate of 1 m/s, whilst the other sample was held stationary (see Hirose and Shimamoto³⁵ for further detail of apparatus and method). After the test, the sample was cut and a thin section was prepared.

Testing the stability of volatiles in the dome rock at eruptive temperature

We conducted complementary experiments to test the ability of the rock to vesiculate at high temperature to ensure that foaming observed in the friction experiments results from the very high-temperatures achieved during fault slip, instead of simply because the rock used contains a concentration of water (quenched-in at high pressure) higher than that which is stable at atmospheric pressure. For this purpose, two small, 8 mm x 8 mm cylindrical samples were heated to a magmatic temperature of 850 °C and one was let to dwell for 30 minutes whilst the other was let to dwell for 15 hours. After the experiment, the samples were cut, polished and carbon coated for SEM analysis.

References

- 34 Petruk, W. Applied Mineralogy in the Mining Industry. 1st edn, 268 (Elsevier, 1990).
- 35 Hirose, T. & Shimamoto, T. Growth of molten zone as a mechanism of slip weakening of simulated faults in gabbro during frictional melting. Journal of Geophysical Research-Solid Earth 110, doi:10.1029/2004jb003207 (2005).

Supplementary Figure 1. Grain size distribution of 3 volcanic ash samples collected during November 2012. At this proximal sampling location (275 m from the vent), most of the ash recovered is below 200 μm in size and the dominant grain size peaks at around 50 μm . The measurements were made using a laser diffraction particle size analyser from Coulter.

Supplementary Figure 2. Back-scattered electron image showing the different phases present in the eruptive products at Caliente. The dome rocks and the volcanic ash samples contain primarily plagioclase (Pl, dark grey), pyroxene (Px, mildly grey), iron oxides (Ox, light grey), apatite (Ap, very dark grey) and interstitial glass (Gl, dark grey). Note the absence of vesicles (black, rounded pores) in this dense ash fragment, which contains less than 2% pore space. Despite the fact that there are no vesicles in this ash particle, we note that the edge of the iron oxides and pyroxene crystals are not straight, but rather crenulated and somewhat diffuse.

Supplementary Figure 3. Back-scattered images showing heterogeneous melt filaments present in volcanic ash erupted at Caliente on a-b) 13 November 2012, and c) 26 November 2014. The yellow box in (a) defines the region of interest displayed in (b). Evidence for high thermal input is best represented by the occurrence of frictional melting. The characteristic texture of frictional melting has been noted in a number of volcanic ash particles and from several eruptions (the main text refers to ash from 10 November 2012). The textures associated with frictional melting preserved in the ash erupted on 13 November 2012 and 26 November 2014, suggest that this dynamic of strain localisation in magma was active for at least two years.

Supplementary Figure 4. Energy-dispersive x-ray spectroscopy (EDS) images showing the heterogeneous concentration of various elements in the melt filaments. a) Back-scattered electron image showing the area mapped by EDS. EDS maps show the distribution of b) Fe (in green), c) Ti (in blue), and d) Al (in red). Colour scale values represent x-ray counts per pixel for each energy band. During frictional melting of andesite and dacite, selective melting tends to affect the iron-titanium oxides more readily than silicate mineral phases due to their lower fusion temperature³⁰.

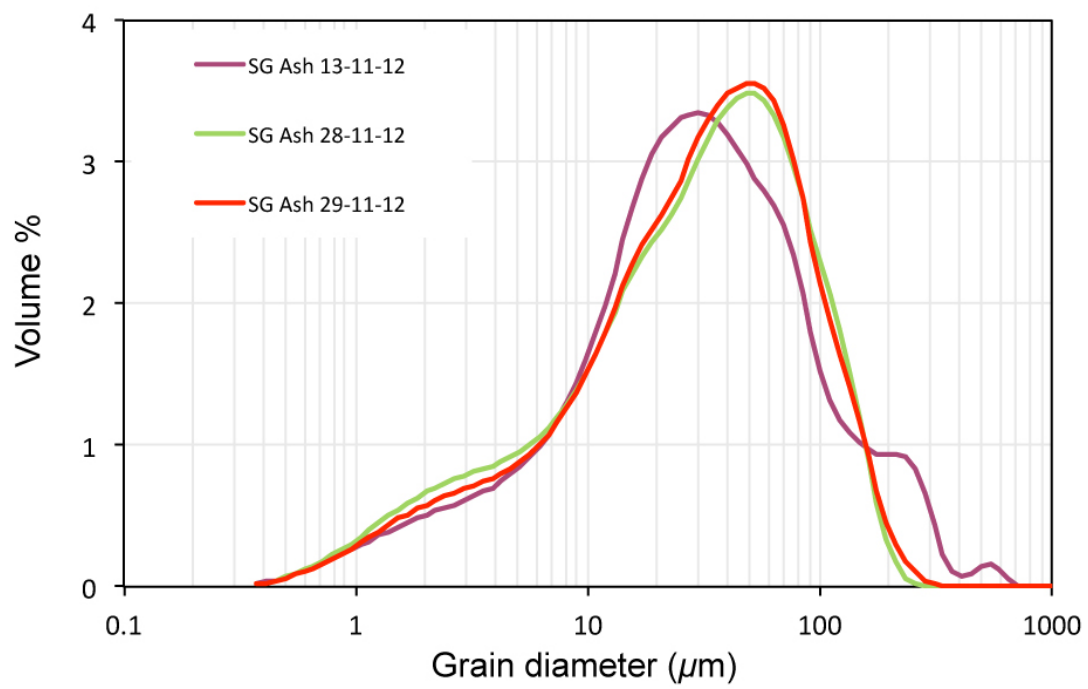
Supplementary Figure 5. Sample assembly setup during rotary shear experiments. The sketch also highlights the area sliced for thin section preparation.

Supplementary Figure 6. Frictional melt chemistry. a) Back-scattered electron image of the different phases and textures observed in the products of the rotary shear experiments, along with eight numbered locations of geochemical analyses acquired with the EPMA and presented in b) the table of normalised geochemical composition of major elements. Comparison of the chemical analyses with the textures reveals the variable heterogeneity of the rock products by frictional melting. Analyses #1 and #2 present pyroxene crystals in the seemingly undisturbed host rock and as fragments in the melt zone respectively; they do not show any degree of contamination. Similarly, #3 presents a Fe-oxide crystal and #6 and #8 present plagioclase crystals in the host rock which have not been chemically altered by the products of frictional melting. #4 presents a protomelt consisting of orthopyroxene with high concentration of Fe-oxide. #5 also presents a protomelt but this time the chemical composition, and in particular the intermediate concentrations of MgO, CaO and FeO, suggests that it is a mixing products of molten plagioclase and orthopyroxene crystals in a ratio nearing 1:1. #7 presents the geochemistry of the more homogenised central frictional melt zone, resulting from the mixing of the molten crystals described above.

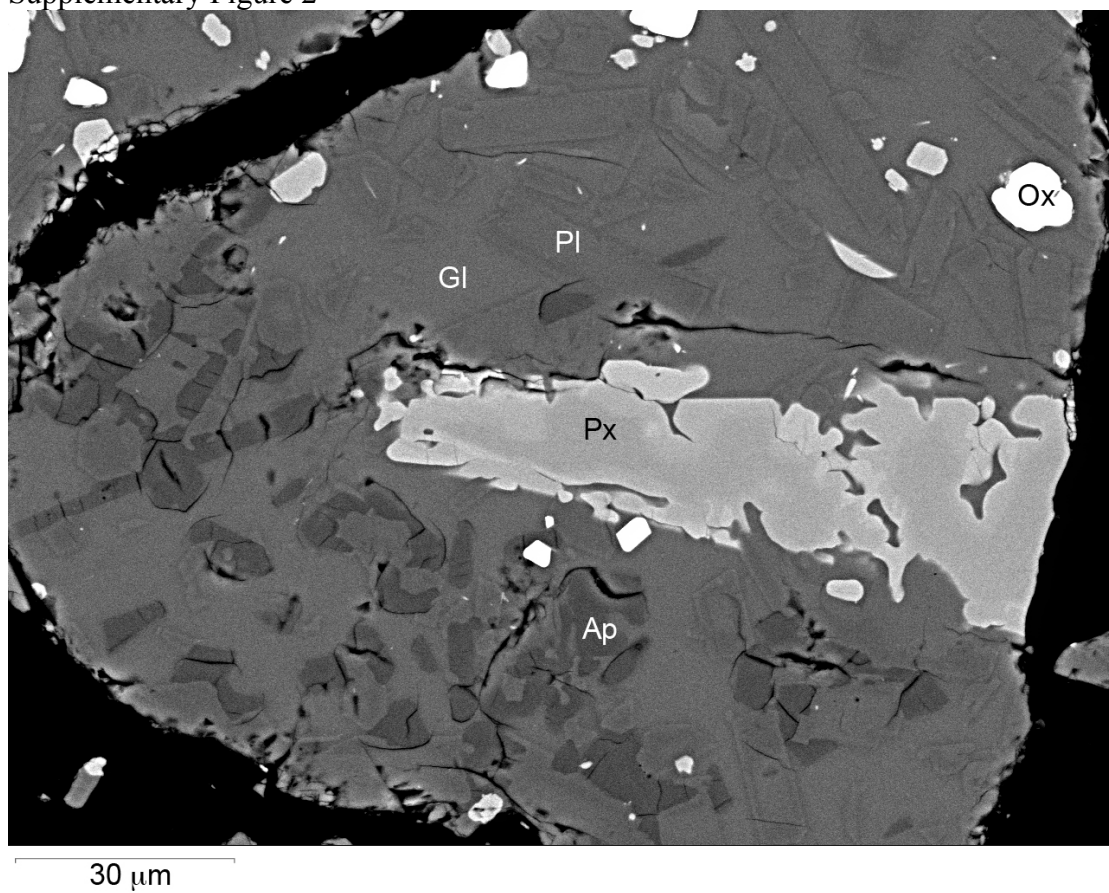
Supplementary Figure 7. Vesicularity (blue arrows) gradient developed in the interstitial glass along the edge of the frictional melt zone (FMZ). We observe no vesicles in the interstitial glass away (>0.4 mm) from the slip zone, and hence no vesicles in the pre-experimental sample.

Supplementary Figure 8. SEM images showing the texture of dome rocks unchanged from subjecting them to 850 °C for a) 30 minutes and b) 15 hours. In either case, we note no new, spherical vesicles developed in the interstitial glass. This observation is consistent with the fact that the sample density did not change, as determined by helium pycnometry. This observation indicates that even at atmospheric pressure, water is unable to exsolve at magmatic temperature, suggesting that high heat input is necessary to lower the solubility and increase diffusivity to trigger vesiculation.

566 Supplementary Figure 1

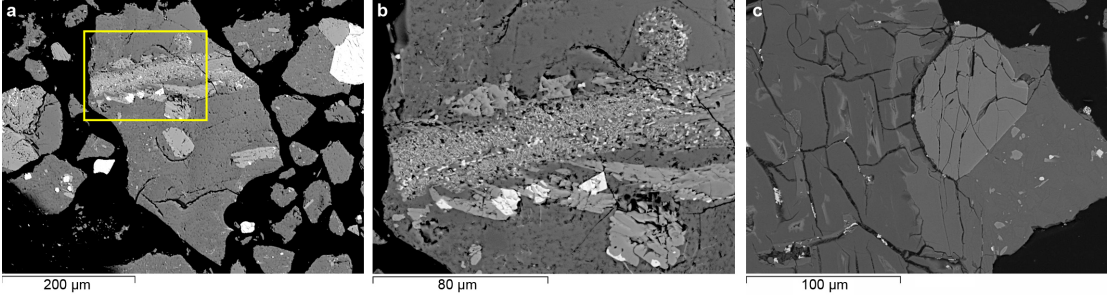


567
568
569 Supplementary Figure 2

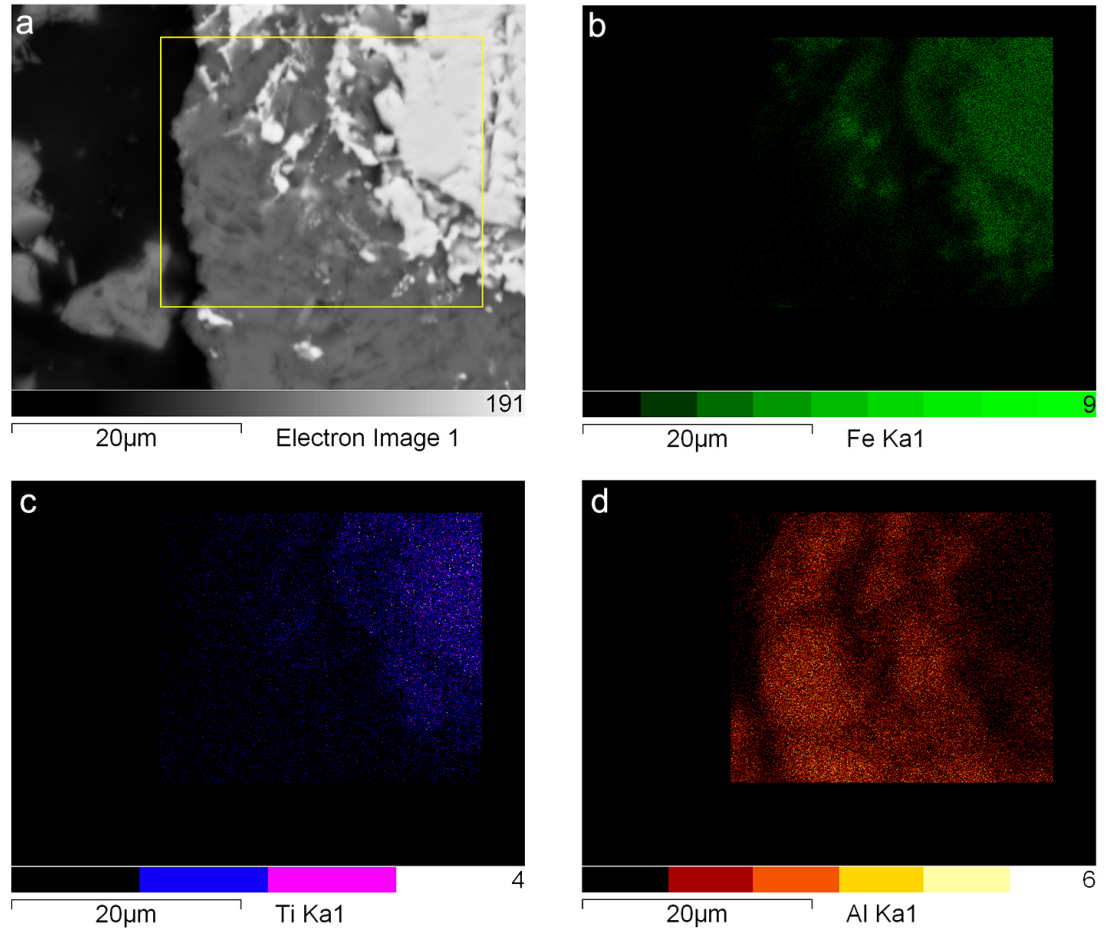


570
571

Supplementary Figure 3

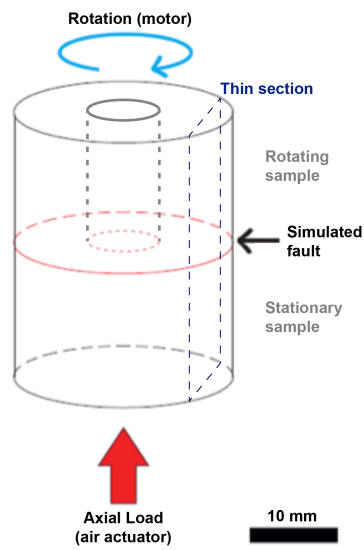


Supplementary Figure 4



578

Supplementary Figure 5

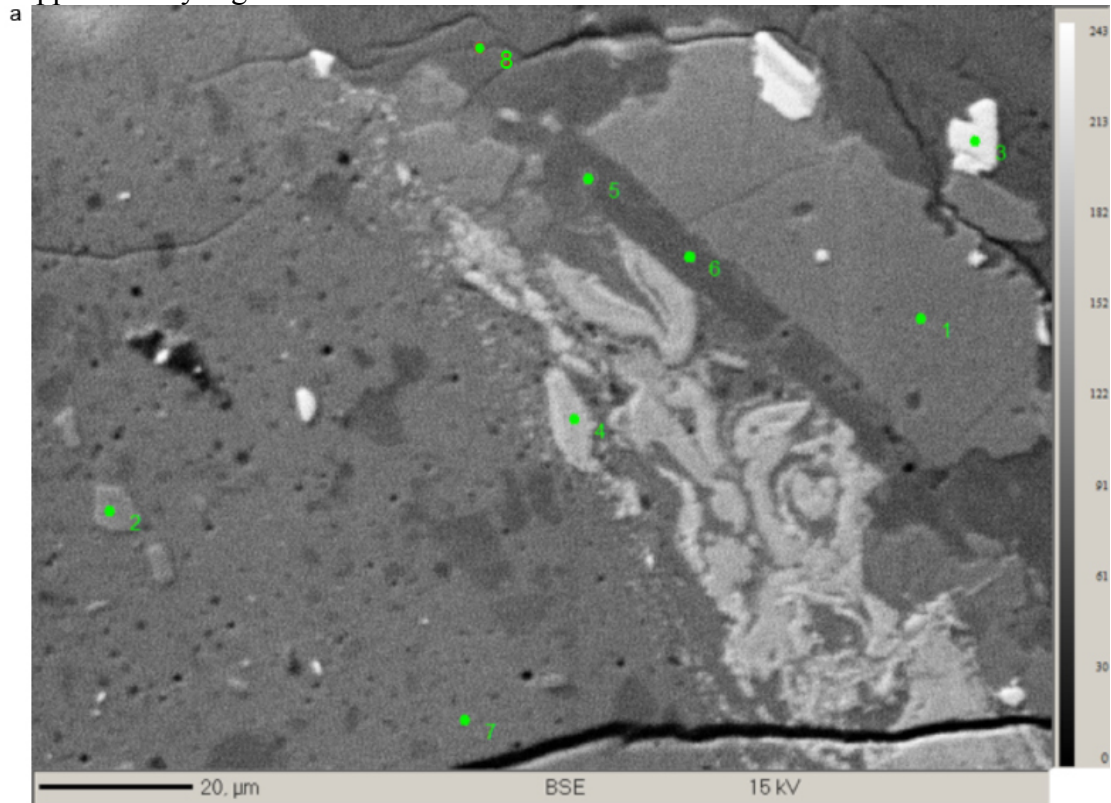


579

580

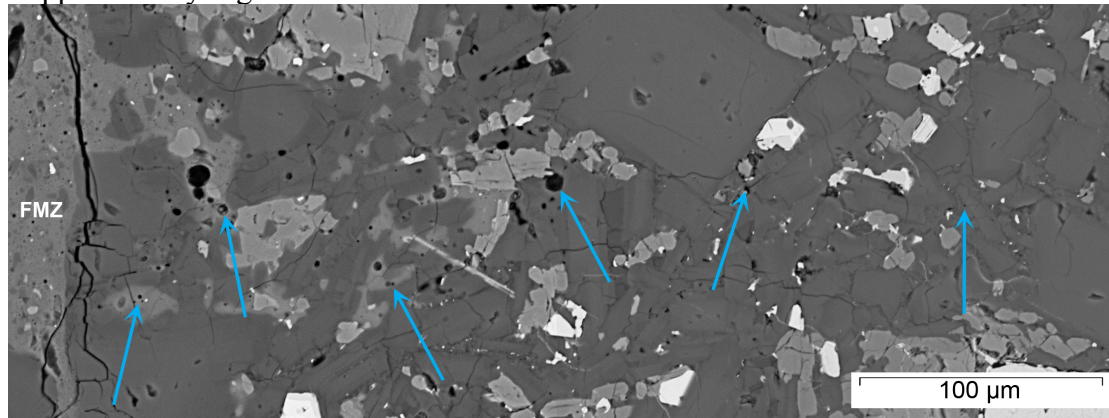
581

Supplementary Figure 6

[illegible]

582

Supplementary Figure 7



Supplementary Figure 8

